


Staggered flux state for rectangular-lattice spin- $\frac{1}{2}$ Heisenberg antiferromagnets

N. E. Shaik ¹, B. Dalla Piazza,¹ D. A. Ivanov,² and H. M. Rønnow¹

¹*Ecole Polytechnique Fédérale de Lausanne (EPFL), Institute of Condensed Matter Physics, CH-1015 Lausanne, Switzerland*

²*Institute for Theoretical Physics, ETH Zürich, CH-8093 Zürich, Switzerland*



(Received 11 May 2020; revised 15 October 2020; accepted 18 November 2020; published 14 December 2020)

We investigate the spin- $\frac{1}{2}$ Heisenberg model on a rectangular lattice, using the Gutzwiller projected variational wave function known as the staggered flux state. Using Monte Carlo techniques, the variational parameters and instantaneous spin-spin correlation function for different coupling anisotropies $\gamma = J_y/J_x$ are calculated. We observe a gradual evolution of the ground state energy towards a value which is very close to the one-dimensional (1D) estimate provided by the Bethe ansatz and a good agreement between the finite-size scaling of the energies. The spin-spin correlation functions exhibit a power-law decay with varying exponents for different anisotropies. Though the lack of Néel order makes the staggered flux state energetically unfavorable in the symmetric case $\gamma = 1$, it appears to capture the essence of the system close to 1D. Hence we believe that the staggered flux state provides an interesting starting point to explore the crossover from quantum disordered chains to the Néel ordered two-dimensional square lattices.

DOI: [10.1103/PhysRevB.102.214413](https://doi.org/10.1103/PhysRevB.102.214413)

I. INTRODUCTION

The Heisenberg interaction constitutes a major type of magnetic interaction between the spins in many materials. It emerges naturally in highly correlated materials with a large Coulomb repulsion. In the field of quantum magnetism, models in various dimensions, involving both ferromagnetic and antiferromagnetic interactions, have been extensively studied. Perhaps one of the most interesting models is the two-dimensional quantum square lattice Heisenberg antiferromagnet which, despite its simplicity, lacks an exact analytical solution. One of the key motivations behind studying this model is because it describes the functional building blocks of parent compounds of high-temperature superconductors like cuprates [1,2], and magnetic fluctuations are speculated to be a reason for the pairing mechanism of the Cooper pairs [3]. At zero temperature, the ground state has antiferromagnetic long-range order with algebraically decaying transverse correlations. The low-energy excitation spectrum consists of magnon excitations described by spin-wave theory [4,5]. However, inelastic-neutron-scattering studies on these structures have shown a striking anomaly at the $(\pi, 0)$ k point that could not be explained using conventional spin-wave theory [6,7]. The main feature of this anomaly is the loss of almost half of spectral weight in the magnon branch, which emerges as a high-energy continuum.

This issue led to the work by Dalla Piazza *et al.* [8], where it was shown that the staggered flux (SF) state [9], a variant of resonating valence bond state, is capable of capturing the essential features of the quantum anomaly. The interesting aspect of this work is that the observed excitations at the quantum anomaly are two-dimensional (2D) analogs of particles carrying fractional ($S = 1/2$) quantum numbers termed as “spinons.” Spinons are the fundamental excitations found in the exact one-dimensional (1D) solution through Bethe ansatz [10] which have experimentally been observed

[11–13]. In higher dimensions, they are proposed to be found mostly in frustrated lattices capable of hosting a quantum spin liquid [14], a disordered phase with high degeneracy at $T = 0$. On the other hand, quasi-1D systems called spin ladders have exhibited experimental features where the low-energy bands are magnonlike and high-energy features are spinonlike [15]. Theoretical work on weakly coupled chains, along with frustrating next-nearest-neighbor couplings, were found to be exhibiting a spinon continuum along with triplon bound states [16]. Contrary to the spinon picture, an alternate proposal by Powalski *et al.* [17,18], based on continuous similarity transformation of the Hamiltonian in momentum space, attributes the $(\pi, 0)$ anomaly to higher order magnon-magnon interaction denoted as magnon-Higgs-like scattering.

Motivated by the work by Dalla Piazza *et al.* [8], we extend their methodology to the rectangular lattice, where by tuning the ratio of spin couplings in the two lattice directions we can interpolate between the square-lattice limit (where spinons are only conjectured at one wave vector in the magnon band) and one-dimensional chains (where spinons are elementary excitations at all wave vectors). Research works relating to such an interpolation between the 1D and 2D are not new. A rich discussion on the nature of the ground state of the 2D Hubbard model took place in the early 1990s, with Luttinger liquid and Fermi liquid being two distinct fixed points. Anderson’s work [19,20] proposed Luttinger-liquid behavior in two-dimensional systems in which the band spectrum is bounded above. Other research works [21,22] showed that Fermi-liquid behavior survives in 2D, at least in the low-density regime. Finally, a dimensional crossover from Fermi to Luttinger liquid was explored by Castellani *et al.* [23], where they proposed a tomographic Luttinger description of this crossover. Though this discussion is related to the charge sector of the Hubbard model, an interesting parallel could be drawn towards the spin sector of the Heisenberg model

($U \rightarrow \infty$), where a disordered quantum spin liquid in 1D and an ordered Néel state in higher dimensions are two distinct solutions.

In this work, preliminary studies of the projected staggered flux wave functions on a rectangular lattice are reported. We compute the variational energies and the spin correlations as a function of the anisotropy parameter. We also comment on the finite-size effects which are especially important in the strongly anisotropic case. These results will be of future use for the analysis of spin excitations in such states. Our work is related to that of Miyazaki *et al.* [24], who studied a similar variational ansatz in the Schwinger-boson construction. Due to the difference in the particle statistics (fermion vs bosons), we do not expect exact agreement between the wave functions in their work and in ours. Furthermore, in view of applying our wave function to the spinon deconfinement problem along the lines of Dalla Piazza *et al.* [8], we do not include antiferromagnetic ordering in our ansatz.

II. METHOD

We consider the Heisenberg Hamiltonian on the rectangular lattice

$$\mathcal{H} = \sum_{\langle i,j \rangle} J_{ij} \mathbf{S}_i \cdot \mathbf{S}_j, \quad (1)$$

where \mathbf{S}_i , \mathbf{S}_j are the spin- $\frac{1}{2}$ operators on nearest-neighbor sites $\langle i, j \rangle$. The coupling J_{ij} is equal to J_x in the x direction and to J_y in the y direction. Without loss of generality, we choose $J_y \leq J_x$ so that the anisotropy parameter $\gamma = J_y/J_x$ lies between 0 and 1.

Following the usual variational procedure for Gutzwiller-projected wave functions [25,26], we consider the ground state $|\psi_{SF}\rangle$ of the auxiliary (“mean-field”) Hamiltonian

$$H_{SF} = - \sum_{\langle i,j \rangle, \sigma} \chi_{ij} c_{i\sigma}^\dagger c_{j\sigma}, \quad (2)$$

where $c_{i\sigma}^\dagger$ and $c_{i\sigma}$ are spin- $\frac{1}{2}$ fermion creation and annihilation operators and the parameter $\chi_{ij} = J_{ij} \langle c_{i\sigma}^\dagger c_{j\sigma} \rangle$. We then optimize these parameters χ_{ij} within a certain symmetry class to minimize the variational energy

$$E = \langle \text{GS} | \mathcal{H} | \text{GS} \rangle \quad (3)$$

of its projected ground state

$$|\text{GS}\rangle = P_{D=0} |\psi_{SF}\rangle, \quad (4)$$

where the operator $P_{D=0}$ projects onto states with exactly one fermion per site.

We restrict our study to the staggered flux ansatz for χ_{ij} (see, e.g., Refs. [9,27]) with different amplitudes in the x and y directions:

$$\chi_{i,i+x} = \chi_x e^{i(-1)^{i_x+i_y} \varphi/4}, \quad \chi_{i,i+y} = \chi_y e^{-i(-1)^{i_x+i_y} \varphi/4}. \quad (5)$$

Due to the projection, there is a redundancy in the phase of the fermion on each site, and the projected state, Eq. (4), only depends on the total flux φ through a lattice cell but not on the distribution of the flux over phases of individual hopping amplitudes χ_{ij} in Eq. (5). Also, the overall normalization of χ_{ij} has no effect on the wave function. The variational wave

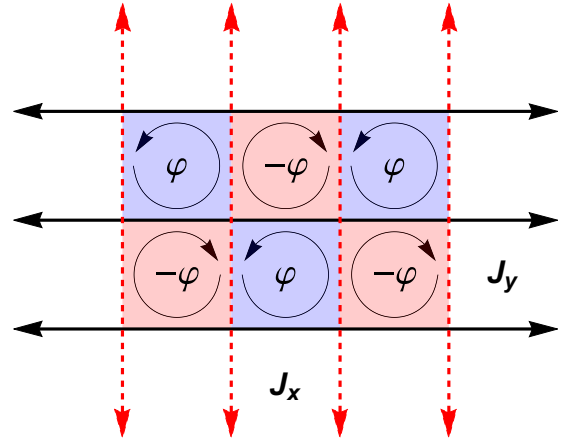


FIG. 1. An illustration of staggered flux state with anisotropic couplings, represented as flux φ threading the lattice in a staggered manner.

function thus depends on two parameters: the flux φ and the hopping anisotropy

$$\alpha = \chi_y / \chi_x. \quad (6)$$

Note that there is a larger symmetry in the particle-hole space that makes our projected staggered flux state identical to a corresponding projected d -wave superconducting state. It has, in fact, been shown that both are related via a $SU(2)$ transformation [28]. For the same reason, the projected staggered flux state |GS) has a full translational symmetry, even though the unprojected state $|\psi_{SF}\rangle$ does not (Fig. 1).

The spectrum of the auxiliary Hamiltonian, Eq. (2), is gapless with nodes at the wave vector $(\pm\pi/2, \pm\pi/2)$ and energy given by

$$\varepsilon_k^\pm = \pm \frac{1}{2} |\chi_x e^{i\varphi/4} \cos k_x + \chi_y e^{-i\varphi/4} \cos k_y|. \quad (7)$$

The ground state wave function corresponds to filling the lower band within the magnetic Brillouin zone (MBZ) with up and down spins,

$$|\psi_{SF}\rangle = \prod_{k \in \text{MBZ}} d_{k\uparrow}^\dagger d_{k\downarrow}^\dagger |0\rangle, \quad (8)$$

where the operators d (d^\dagger) are the annihilation (creation) operators for the eigenstates of the Hamiltonian, Eq. (2).

The observables in the projected state, Eq. (4), are calculated as

$$\langle \text{GS} | O | \text{GS} \rangle = \frac{\langle \psi_{SF} | P_{D=0} O P_{D=0} | \psi_{SF} \rangle}{\langle \psi_{SF} | P_{D=0} | \psi_{SF} \rangle}. \quad (9)$$

Considering a Hilbert space made up of states $|\beta\rangle$ where all the lattice sites are singly occupied, we may write the Gutzwiller projector as $P_{D=0} = \sum_\beta |\beta\rangle \langle \beta|$ and express the expectation value, Eq. (9), as a statistical average:

$$\langle O \rangle = \sum_\beta \frac{|\langle \beta | \psi_{SF} \rangle|^2}{\sum_{\beta'} |\langle \beta' | \psi_{SF} \rangle|^2} \left(\sum_\gamma \langle \beta | O | \gamma \rangle \frac{\langle \gamma | \psi_{SF} \rangle}{\langle \beta | \psi_{SF} \rangle} \right). \quad (10)$$

The above equation has the form of a weighted average of a function $f(\beta)$ with $\rho(\beta)$ being its normalized probability

distribution. The space $\{|\beta\rangle\}$ has a size of 2^N where N is the number of sites and hence we cannot calculate exactly the expectation value using Eq. (10). Therefore we use a Monte Carlo algorithm for this purpose [25]. We start the walk with a state $|\beta\rangle$, initialized through randomly filling up and down spins in the position space, and derive a new state $|\beta'\rangle$ at each step by flipping a pair of randomly chosen spins. At each step, the new overlap amplitude $|\langle\beta'|\psi_{SF}\rangle|^2$ given by a Slater determinant is calculated. The ratio between the new and old overlap amplitudes is used as the acceptance ratio. After every N steps, a measurement of the function $f(\beta)$, as defined in Eq. (10), is performed by calculating the matrix elements $\langle\beta|O|\gamma\rangle$ and the overlap $\langle\gamma|\psi_{SF}\rangle$. In principle, the sum runs over all states $|\gamma\rangle$ in the single-occupancy basis, but since we are only interested in averaging local operators O (such as energy or static spin structure factor), for a given $|\beta\rangle$ there are only a few relevant $|\gamma\rangle$ states with nonzero $\langle\beta|O|\gamma\rangle$. For calculating the energy, the operator O is the physical Hamiltonian, Eq. (1).

III. RESULTS

A. Variational energy

The first step of the calculation is optimizing the values of variational parameters α and φ by finding the minimum energy of the variational state. Figure 2 shows the energy maps in (φ, α) parameter space at $\gamma = \{0.1, 0.2, 0.5, 1\}$ for system size $L = 8$. At large γ , the minima are well defined, but closer to $\gamma \sim 0$ the minima become shallow in φ . This comes as no surprise, since when approaching the 1D case, the notion of flux around a loop is ill-defined.

The ground state energies and the corresponding optimum parameters, for system sizes $L \times L$ with $L = \{8, 12, 16, 24\}$, were extracted by fitting the low-energy part of the maps with a quadratic function in φ and α . The optimum parameters and energy at the system size $L = 24$ are shown in Fig. 3. The ground state energy is compared with the variational work by Miyazaki *et al.* [24] using Gutzwiller-projected Schwinger boson states (SBGP), Quantum Monte Carlo [29,30] (QMC), and spin-wave theory (SWT) [31] including the linear part and next order corrections. Starting from the symmetric case $\gamma = 1$, we observe that the staggered flux state has higher energy compared to all three methods. The energy difference decreases as the coupling ratio is decreased, and at $\gamma \leq 0.1$ we observe the SF state outperforming the SBGP result. With decreasing γ , the flux parameter φ increases slightly and the amplitude ratio α decreases. Interestingly, α decreases slower than γ , such that α/γ increases with decreasing γ , as shown in Fig. 3(d).

B. Finite-size analysis

Since our calculations are performed on finite lattices, a finite-size analysis is needed to establish the convergence of our parameters and validate our conclusions for infinite size limit. It must be noted here that our ground state wave function explicitly depends on the phase of the function inside the modulus in Eq. (7), which is ill-defined at the nodal point. To avoid this point, for system sizes $L = 4n$, Dalla Piazza *et al.* [8,32] worked with antiperiodic boundary conditions in x and

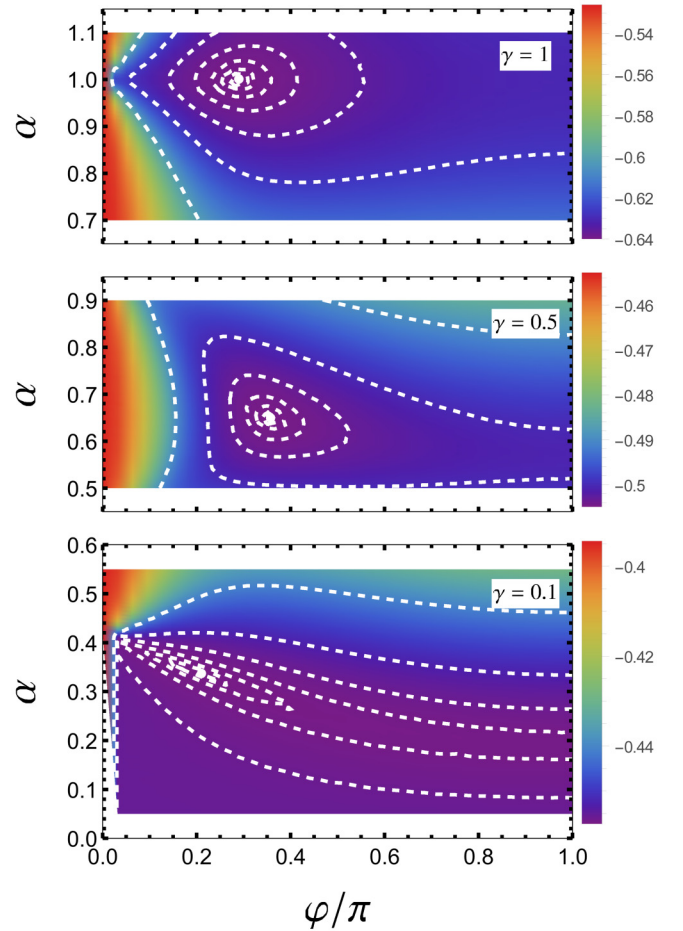


FIG. 2. Ground state energy maps of systems with size $L = 8$ for various coupling ratios. The white contours (dot) indicate the points corresponding to same energy (minima).

y directions, termed here as *abc-abc* (used in Fig. 3). We take this method one step further, by including another possibility, periodic in x and antiperiodic in y (*abc-pbc*).

The advantage of using different boundary conditions is that it provides us with an efficient method to identify features explicitly related to finite system size as opposed to ones that can be extended to $L \rightarrow \infty$. The ground state energy calculations are also performed on system sizes of type $L = 4n + 2$ with boundary conditions *pbc-pbc, abc-pbc*. To save computational cost, optimization routines have not been performed for $L = 4n + 2$ system sizes; instead, the average values of $L = 4n$ and $L = 4n + 4$ parameters were used as input to the variational wave function.

Figure 4 shows the energies corresponding to the mentioned possibilities. To avoid confusion, from here on we refer to the boundary condition only in the x direction, and it is understood that corresponding boundary conditions in the y direction are *abc* for $L = 4n$ and *pbc* for $L = 4n + 2$. From Fig. 4, we can see that the sensitivity to boundary conditions decreases with increasing coupling. A comparison with the energies from Bethe ansatz shows an important observation. For systems $L = 4n$, we observe that our wave functions with *abc*, are closer to the Bethe ansatz with *pbc*, and vice versa. This situation is reversed for $L = 4n + 2$. The observed

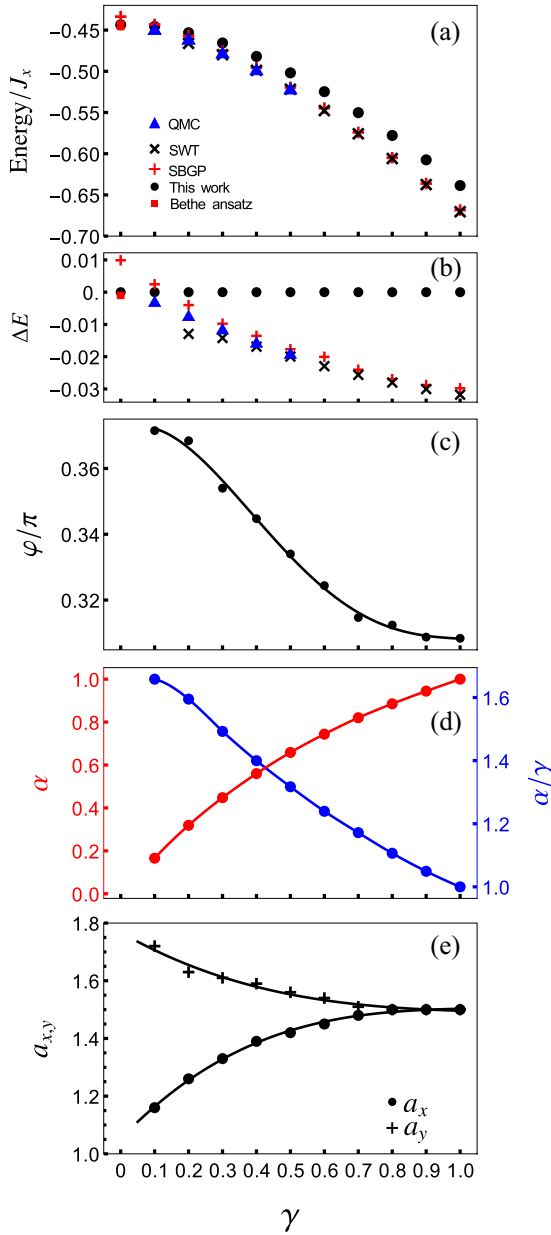


FIG. 3. Properties of the variational wave function as a function of γ . (a) Energies and their (b) differences, compared to quantum Monte Carlo methods (QMC), spin-wave theory (SWT), Gutzwiller-projected Schwinger boson states (SBGP), and Bethe ansatz (at $\gamma = 0$). Optimized variational parameters φ (c) and α (d). (e) Exponents of the algebraically decaying staggered correlation functions. The system size is 24×24 for (a)–(d) and $\gamma \geq 0.6$ in (e). For $\gamma < 0.6$ in (e), system size 56×16 has been used. The lines are guides to the eye.

equivalence between *abc* (*abc*) for $L = 4n + 2$ and *abc* (*abc*) for $L = 4n$ can be easily understood by inspecting the corresponding k space where $k_x = \pi/2$ is avoided (included). The equivalence between *abc* for $L = 4n$ and *abc* for Bethe ansatz is due to the fermionic nature of our wave function, which upon the imposition of translational symmetry incur a sign difference that depends on whether there is an even or odd number of down spins (see Supplemental Material [33]).

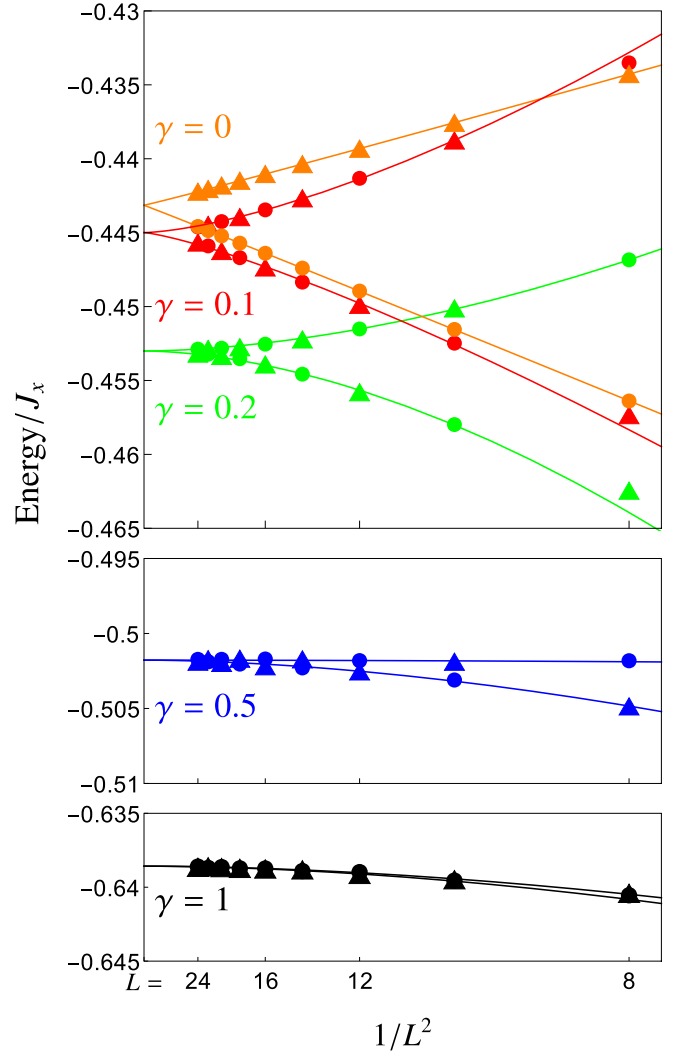


FIG. 4. Finite-size scaling of ground state energies along with the algebraic fitting for selected γ . The plot markers are assigned with respect to boundary condition in the x direction representing *abc* (*pbc*) with triangles (circles). The $\gamma = 0$ plots and fits correspond to exact solution using Bethe ansatz.

C. Instantaneous spin correlation

Next, we calculate the instantaneous staggered spin-spin correlation function $S^{\alpha\alpha}(r) = 1/N \sum_i e^{iQr} \langle S_{i+r}^\alpha S_i^\alpha \rangle$ with $Q = (\pi, \pi)$. In the absence of symmetry breaking long-range order, $S^{xx}(r)$, $S^{yy}(r)$, and $S^{zz}(r)$ are equivalent. Numerically, we observe that the xx component converges faster than the zz component (see Supplemental Material [33]). Starting with the x direction, as can be seen in Fig. 5(a), $S^{xx}(x)$ decays as a power law. At large γ , the correlation functions are insensitive to the boundary conditions, while at small γ (e.g., $\gamma = 0.1$), deviations appear noticeable at large r . This is solved by increasing system size. As shown for $S^{xx}(x)$ at $\gamma = 0.1$ in Fig. 5(b), when increasing L_x with $L_y = 16$, the correlation functions converge. Interestingly, as can be seen from the slopes in Fig. 5(a), the exponent a_x in $S^{xx}(x) \propto x^{-a_x}$ appears to vary as a function of γ , as summarized in Fig. 3(e).

Various estimates exist for $S^{xx}(x)$ in the pure 1D case ($\gamma = 0$). The exact values for nearest neighbor [34] (0.147 71)

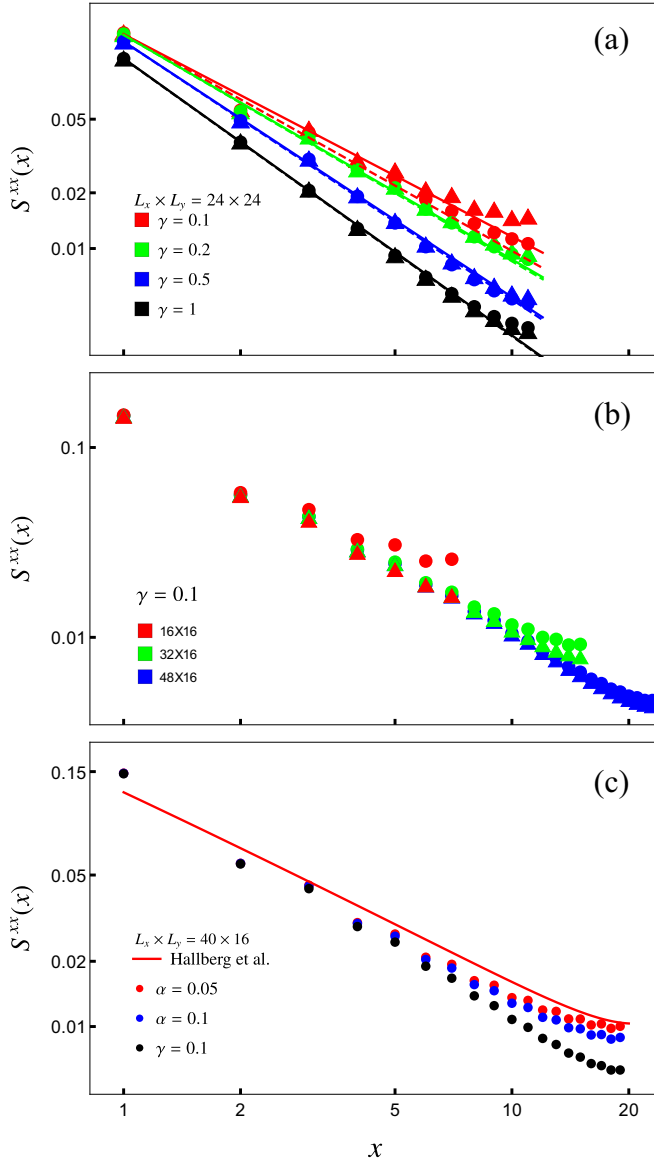


FIG. 5. (a) $S^{xx}(x)$ for $\gamma = 0.1, 0.2, 0.5, 1$ and the corresponding fits to algebraic decay $S^{xx}(x) \propto x^{-\alpha_x}$ at $L = 24$. (b) $S^{xx}(x)$ at $\gamma = 0.1$ for different system sizes. (c) $S^{xx}(x)$ for $\alpha = 0.05, \alpha = 0.1, \gamma = 0.1$ for system size 40×16 compared to the expression from Hallberg *et al.* [37]. The plot markers in (a) and (b) are assigned with respect to the boundary condition in the x direction representing abc (abc) with triangles (circles).

and the next-nearest neighbor [35] (0.06068) are known. From field theory [36] the exact expression at $r \rightarrow \infty$ is $\sqrt{\ln r}/[(2\pi)^{3/2}r]$. Results for finite system sizes have been calculated through density matrix renormalization group (DMRG) methods [37]. To compare with these results, we calculate the correlation function at $\gamma \sim 0$ for larger system sizes $L_x \times L_y = 40 \times 16$. Optimizing the variational parameters for $\gamma < 0.1$ is challenging since the energy minima are extremely flat in (α, φ) space. We assume that α/γ has a finite value as we approach $\gamma = 0$, and carry out the calculations for small α values. In Fig. 5(c), we present the results for $\alpha = 0.05, 0.1$ and also for the optimized wave function at $\gamma = 0.1$. The nearest- and next-nearest-neighbor values at $\alpha = 0.05$ are

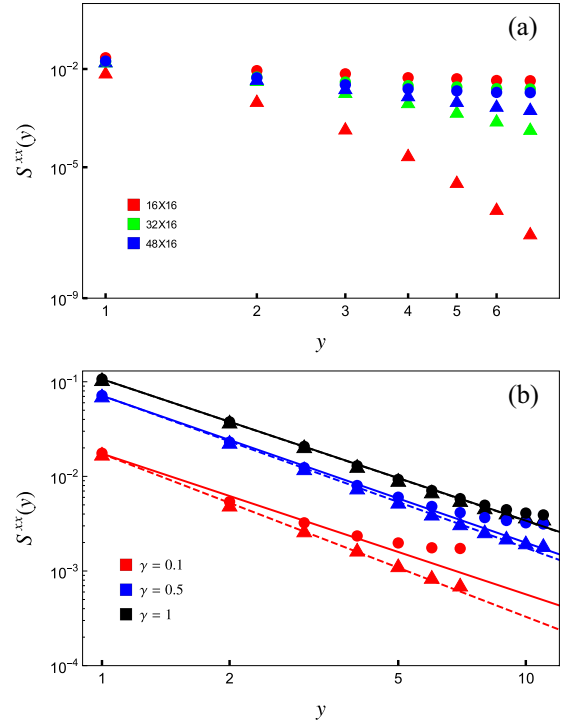


FIG. 6. (a) Sensitivity of correlations in the y direction to the boundary conditions at $\gamma = 0.1$ for different system sizes. (b) Correlations in the y direction for couplings $\gamma = 0.1, 0.5, 1$ and the corresponding fits to algebraic decay $S^{yy}(y) \propto y^{-a_y}$ at $L = 24$. The plot markers are assigned with respect to the boundary condition in the x direction representing abc (abc) with triangles (circles).

0.1475 and 0.05662, close to the exact values. A comparison with the DMRG result from the work of Hallberg *et al.* [37] shows that our correlation functions at $\gamma \sim 0$ progressively get closer to the 1D estimate as we reduce the coupling ratio γ .

Along the y direction, the correlation function becomes very sensitive to boundary conditions for small γ . Interestingly, the remedy is to increase system size along the strong-coupling x direction as shown in Fig. 6(a). Similar to the x direction, the correlation functions remain algebraic, however with an exponent a_y that increases with decreasing γ . The extracted exponents are plotted in Fig. 3(e), and the values are provided in the Supplemental Material [33]. For $\gamma \geq 0.6$, where the differences between abc and abc are negligible, system size 24×24 is used to extract the exponents through fitting by power law. For $\gamma < 0.6$, to achieve convergence of correlation functions for different boundary conditions, a system size of 56×16 has been used.

The fact that a_y increases and a_x decreases with decreasing γ would imply that as coupling between chains weakens, correlations decay faster across chains, but decay slower along the chain than in the 2D square lattice case. We note that the exponents extracted here are fits of up to 12 lattice spacing. It is possible that the asymptotic exponents in the large distance limit would behave differently, for instance converge to a universal gamma independent value.

IV. DISCUSSION

Our work focuses on extending the staggered flux variational wave-function approach to rectangular lattices, and the ground state properties of this wave function have been presented in this paper. In the main part of the paper, we have compared our results with other methods, and in this section we discuss the key conclusions on this comparison. Starting with the ground state energy, for large γ , our estimates are higher than the QMC [29], SBGP [24], and SWT results [31]. This is not surprising, and has been already noted by Dalla Piazza *et al.* [8,32]. A disordered staggered flux state for the square lattice has higher energy ($-0.638J$) compared to an ordered staggered flux state ($-0.664J$) and the current best estimate by the Green's function Monte Carlo method ($-0.669J$) [38–40]. However, they also note that, although the ordered staggered flux state performs better energetically, it does not reproduce the quantum anomaly, exhibits a gapped spectrum, and has exponentially decaying spin-spin correlations contrary to the expected power-law decay.

On the other end of the coupling ratio is the quasi-1D case $\gamma \rightarrow 0$ where the staggered flux wave function energetically performs better than the SBGP state but has slightly higher energy than the QMC result. To estimate the energy in the pure 1D case, Miyazaki *et al.* [24] set $J_y = 0$ and treat γ as a variational parameter, and the optimum result yields $E(\gamma = 0) = -0.4337$ at $L = 20$. Using a similar logic, at $L = 20$ we set $\gamma = 0$ and calculate the energy of a state with very small $\alpha = 0.05$. This yields a value of $E(\gamma = 0) = -0.4442$, which is very close to the exact value from Bethe ansatz $E(\gamma = 0, L = 20) = -0.4445$. Extrapolating the $[E(L = \infty)]$ values from Fig. 4 through a third-order polynomial fit (see Supplemental Material [33]), we obtain the 1D estimate at infinite system size $E(L = \infty, \gamma = 0) = -0.4414$, a value very close to the

Bethe ansatz estimate of -0.4431 . Some research works using mean-field theories, suggest that from the limit of coupling spin chains, long-range order sets in already at infinitesimal interchain coupling [41,42]. On the other hand, the ordered moment calculations through spin-wave theory (with first correction) reaches zero for $\gamma = 0.138$, below which spin-wave theory breaks down [31]. This suggests that a disordered phase exists for a finite γ , a result discussed by Parola *et al.* [43]. Though a similar observation was made through a mean-field treatment by Miyazaki *et al.* [24], where the ordered moment goes to zero at a value $\gamma = 0.1356$, the analysis of the SBGP state at $\gamma = 0$ seems to indicate that long-range order exists all the way down to $\gamma = 0$. This suggests that the loss of order at $\gamma \sim 0.138$ is just an artifact of the mean-field methodologies. Interestingly, in our work at $\gamma \leq 0.1$, the ground state energy of the staggered flux state is lower than the SBGP result. This indicates that, although the staggered flux result at $\gamma = 0.1$ falls short of outperforming the QMC result, within the framework of variational wave functions, the staggered flux fermionic wave function outperforms the bosonic SBGP wave function.

In conclusion, while the staggered flux state is compromised by lacking Néel order, it appears to capture the essence of the system at low γ . We therefore believe the presented staggered flux state provides an interesting starting point for exploring the crossover from quantum disordered chains to the Néel ordered 2D square lattices.

ACKNOWLEDGMENT

We would like to thank Bowen Zhao and Anders W. Sandvik for the sharing the QMC data included in Fig. 3.

-
- [1] J. G. Bednorz and K. A. Müller, *Z. Phys. B* **64**, 189 (1986).
 - [2] M. Buchanan, *Nature (London)* **409**, 8 (2001).
 - [3] P. Monthoux, A. V. Balatsky, and D. Pines, *Phys. Rev. Lett.* **67**, 3448 (1991).
 - [4] P. W. Anderson, *Phys. Rev.* **86**, 694 (1952).
 - [5] R. Kubo, *Phys. Rev.* **87**, 568 (1952).
 - [6] H. M. Rønnow, D. F. McMorrow, R. Coldea, A. Harrison, I. D. Youngson, T. G. Perring, G. Aeppli, O. Syljuåsen, K. Lefmann, and C. Rischel, *Phys. Rev. Lett.* **87**, 037202 (2001).
 - [7] N. B. Christensen, H. M. Rønnow, D. F. McMorrow, A. Harrison, T. G. Perring, M. Enderle, R. Coldea, L. P. Regnault, and G. Aeppli, *Proc. Natl. Acad. Sci. USA* **104**, 15264 (2007).
 - [8] B. Dalla Piazza, M. Mourigal, N. B. Christensen, G. J. Nilsen, P. Tregenna-Piggott, T. G. Perring, M. Enderle, D. F. McMorrow, D. A. Ivanov, and H. M. Rønnow, *Nat. Phys.* **11**, 62 (2014).
 - [9] J. B. Marston and I. Affleck, *Phys. Rev. B* **39**, 11538 (1989).
 - [10] H. Bethe, *Z. Phys.* **71**, 205 (1931).
 - [11] D. A. Tennant, R. A. Cowley, S. E. Nagler, and A. M. Tsvelik, *Phys. Rev. B* **52**, 13368 (1995).
 - [12] B. Lake, D. A. Tennant, C. D. Frost, and S. E. Nagler, *Nat. Mater.* **4**, 329 (2005).
 - [13] M. Mourigal, M. Enderle, A. Klöpperpieper, J.-S. Caux, A. Stunault, and H. M. Rønnow, *Nat. Phys.* **9**, 435 (2013).
 - [14] L. Balents, *Nature (London)* **464**, 199 (2010).
 - [15] B. Lake, A. M. Tsvelik, S. Notbohm, D. Alan Tennant, T. G. Perring, M. Reehuis, C. Sekar, G. Krabbes, and B. Büchner, *Nat. Phys.* **6**, 50 (2009).
 - [16] M. Kohno, O. A. Starykh, and L. Balents, *Nat. Phys.* **3**, 790 (2007).
 - [17] M. Powalski, G. S. Uhrig, and K. P. Schmidt, *Phys. Rev. Lett.* **115**, 207202 (2015).
 - [18] M. Powalski, K. P. Schmidt, and G. S. Uhrig, *SciPost Phys.* **4**, 001 (2018).
 - [19] P. W. Anderson, *Phys. Rev. Lett.* **64**, 1839 (1990).
 - [20] P. W. Anderson, *Phys. Rev. Lett.* **65**, 2306 (1990).
 - [21] H. Fukuyama, Y. Hasegawa, and O. Narikiyo, *J. Phys. Soc. Jpn.* **60**, 2013 (1991).
 - [22] J. R. Engelbrecht and M. Randeria, *Phys. Rev. B* **45**, 12419 (1992).
 - [23] C. Castellani, C. Di Castro, and W. Metzner, *Phys. Rev. Lett.* **72**, 316 (1994).
 - [24] T. Miyazaki, D. Yoshioka, and M. Ogata, *Phys. Rev. B* **51**, 2966 (1995).
 - [25] C. Gros, *Ann. Phys.* **189**, 53 (1989).
 - [26] D. V. Dmitriev, V. Y. Krivnov, V. N. Likhachev, and A. A. Ovchinnikov, *Fiz. Tverd. Tela* **38**, 397 (1996) [*Sov. Phys. Solid State* **38**, 219 (1996)].

- [27] D. A. Ivanov and P. A. Lee, *Phys. Rev. B* **68**, 132501 (2003).
- [28] I. Affleck, Z. Zou, T. Hsu, and P. W. Anderson, *Phys. Rev. B* **38**, 745 (1988).
- [29] A. W. Sandvik, *Phys. Rev. Lett.* **83**, 3069 (1999).
- [30] Anders W. Sandvik and B. Zhao (private communication).
- [31] N. E. Shaik, From quantum spin chains to square lattice Heisenberg anti-ferromagnets, EPFL theses, Ecole polytechnique Federale de Lausanne, Lausanne, Switzerland, 2019.
- [32] B. Dalla Piazza, Theories of Experimentally Observed Excitation Spectra of Square Lattice Antiferromagnets, EPFL theses, Ecole polytechnique Federale de Lausanne, Lausanne, Switzerland, 2014.
- [33] See Supplemental Material at <http://link.aps.org/supplemental/10.1103/PhysRevB.102.214413> for additional information.
- [34] L. Hulthén, Über das Austauschproblem eines Kristalles, Ph.D. thesis, Uppsala, 1938.
- [35] M. Takahashi, *J. Phys. C* **10**, 1289 (1977).
- [36] I. Affleck, *J. Phys. A: Math. Gen.* **31**, 4573 (1998).
- [37] K. A. Hallberg, P. Horsch, and G. Martínez, *Phys. Rev. B* **52**, R719 (1995).
- [38] N. Trivedi and D. M. Ceperley, *Phys. Rev. B* **40**, 2737 (1989).
- [39] K. J. Runge, *Phys. Rev. B* **45**, 12292 (1992).
- [40] M. Calandra Buonauro and S. Sorella, *Phys. Rev. B* **57**, 11446 (1998).
- [41] T. Sakai and M. Takahashi, *J. Phys. Soc. Jpn.* **58**, 3131 (1989).
- [42] M. Azzouz, *Phys. Rev. B* **48**, 6136 (1993).
- [43] A. Parola, S. Sorella, and Q. F. Zhong, *Phys. Rev. Lett.* **71**, 4393 (1993).